

# Investigation into Electromechanical Properties of Biocompatible Chitosan-Based Ionic Actuator

Z. Sun<sup>1</sup> · G. Zhao<sup>2</sup> · W.L. Song<sup>1</sup> · J. Wang<sup>2</sup> · M. Ui Haq<sup>2,3</sup>

Received: 9 August 2016 / Accepted: 21 August 2017 / Published online: 28 August 2017  
© Society for Experimental Mechanics 2017

**Abstract** Ionic actuators have attracted much attention due to their remarkably large strain under low-voltage stimulation. Here, we investigate a highly biocompatible ionic polymer actuator, which consists of multi-walled carbon nanotube (MCNT) film as a double electrode layer and an electrolyte layer equipped with chitosan polymer skeleton and ionic liquid. As a result, with the thickness increase of the electrolyte layer and the electrode layer, the membrane capacitance values are obviously improved, which are 0.01 F (membrane thickness of 1.3 mm) and 0.4 F (0.25 mm). The blocking force and its response speed show peak values of 5.75 mN (1.1 mm) and 5.1 mN (0.25 mm), while reverse increases for the displacement and its response speed are observed, which present maximum values of 10.3 mm (0.3 mm) and 13.3 mm (0.15 mm). Furthermore, for various thicknesses of the electrode layers under applied direct current of 5 V, the generated strain of 0.15 mm thickness (59%) is 4.92 times greater than that of the 0.25 mm thickness. This is against the strain difference on the electrode surface due to the growing stiffness of the electrode layer. Additionally, from the experiments of the electromechanical energy efficiency of various electrode layers and electrolyte layers, our actuator exhibits excellent electromechanical energy efficiency under a high electrical

conductivity of the electrode layer, which enhance the specific electromechanical energy up to 9.95%.

**Keywords** Biocompatible · Ionic actuator · Electromechanical properties · Electromechanical energy efficiency

## Introduction

In recent decades, bio-inspired actuation materials, which are also called artificial muscles, have attracted great attention due to their potential applications in intelligent robots, biomimetic devices, and micro-electro-mechanical systems [1–5]. Among these materials, ionic actuators have been intensively studied due to their impressive actuation under low voltage stimulation [6–8]. Typical ionic actuators with a bimorph structure include ionic polymer-metal composites, polymer gels, and carbon nanotubes (CNTs) [9–11]. After several decades of development, their performances have improved greatly to satisfy desired practical industrial applications. Their advantages of low actuation voltages make applications related to human life possible, such as heart compression devices, surgical tools, and ocular muscles [12, 13]. To achieve this goal, biocompatible low voltage actuation materials are desired. A recent significant step is the discovery of an actuator based on the biopolymer chitosan [14–17]. Chitosan, an abundant natural polymer, not only is a lightweight, low-cost, and sustainable resource with potentials application in energy transformation but also demonstrates biocompatibility and biodegradability. Therefore, the possibility of constructing a biocompatible polymer actuator has been demonstrated in some earlier research investigations [18–20].

Furthermore, the supramolecular chemistry of CNTs has attracted great attention in the preparation of a variety of

---

✉ Z. Sun  
sunzhuangzhi@nefu.edu.cn

<sup>1</sup> College of Mechanical and Electrical Engineering, Northeast Forestry University, Harbin 150000, People's Republic of China

<sup>2</sup> College of Mechanical and Electrical Engineering, Harbin Engineering University, Harbin 150000, People's Republic of China

<sup>3</sup> College of Mechanical and Aeronautical Engineering, University of Engineering and Technology, Taxila 47080, Pakistan

anisotropic composite membranes, biosensors, and tissue engineering [21–25]. CNTs non-covalently functionalized by the biopolymer chitosan play an important role in almost all of the mentioned fields and have potential applications in implanted sensors and pacemakers [26–31]. Thus, multi-walled carbon nanotubes (MCNTs) are essential for fabricating the electrode materials of the biopolymer actuator. Additionally, few reports have investigated the electromechanical efficiency of this type of polymer actuator. Most of the related works have concentrated on the improvement of the actuation performance through doping methods, etc. Nevertheless, a unified standard does not exist for evaluating the performance enhancements after a series of chemical modifications.

This manuscript is mainly focused on research regarding the electromechanical properties of a chitosan based polymer (C-polymer) actuator with various thicknesses of the electrolyte layer, which is equipped with a chitosan polymer skeleton and ionic liquid, and various thicknesses of the electrode layer, which consists of MCNTs film as a double electrode layer. After exploring the actuation rules of the electromechanical properties, the electromechanical energy efficiencies of various electrode layers and various electrolyte layers are further obtained to evaluate the effects of performance enhancements.

## Experiments

### Materials

Multi-walled carbon nanotubes (MCNTs) were obtained from Boyu Company (Beijing, China). Chitosan (deacetylation degree of 85.66%, viscosity of 450 mPa·s, Cs powder) was purchased from HaiDebei Marine Bioengineering Company (Jinan, China). Ionic liquid used here was 1-butyl-3-methylimidazolium tetrafluoroborate (BMIBF<sub>4</sub>) (MW = 226.0) (Lanzhou Institute of Physical and Chemistry). Other reagents used were glycerol and acetic acid, etc., from Yongchang Company (Harbin, China). Some chemical structures of the reagents used, such as MCNTs, chitosan, and BMIBF<sub>4</sub>, are shown in Fig. 1(a).

### Preparation of C-polymer Actuator

The configuration of the C-polymer actuator is illustrated in Fig. 1(b). Typically, the polymer-supported electrode layer was composed of MCNTs, BMIBF<sub>4</sub> and Cs, and the polymer-supported electrolyte film consisted of Cs, BMIBF<sub>4</sub> and glycerol. The preparation processes are presented as follows. First, 2 mL of BMIBF<sub>4</sub> and 10 mL of MCNT dispersed solution were added to 15 mL of 2% Cs in acetic acid solution and stirred in a 60 °C water bath. After that, a gelatinous mixture was produced. The electrode layer was fabricated by casting 12 mL of the gelatinous mixture in a glass mould

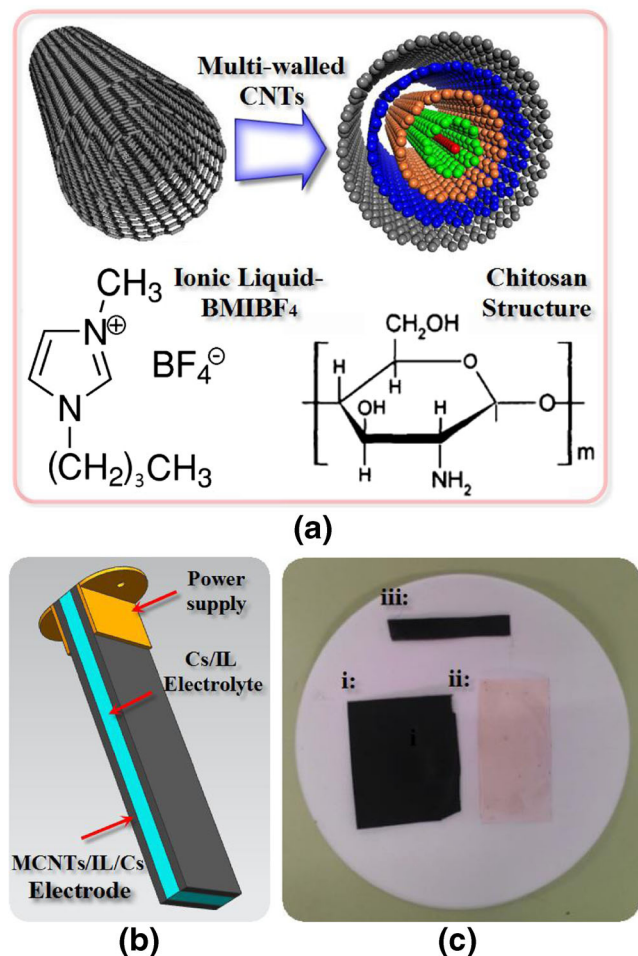


**Fig. 1** (a) Schematic structure of the polymer chitosan (i), ionic liquid-BMIBF<sub>4</sub> (ii), and the three-dimensional structure of multi-walled carbon nanotubes (MCNTs) (iii). (b) Schematic structure of C-polymer actuator strip composed of a chitosan polymer supported ionic liquid electrolyte layer sandwiched by MCNTs electrode layers. (c) Schematic of the fabricated chitosan polymer actuator: MCNTs/IL/Cs electrode film (i), Cs/IL electrolyte film (ii) and C-polymer actuator (iii)

(5 × 5 cm<sup>2</sup>) and placed in air for 30 min. The solvent was then placed in an oven at 60 °C to obtain the electrode film, whose thickness was 40–50 μm. The electrolyte layer was fabricated by adding 2 mL of BMIBF<sub>4</sub> and 1 mL of glycerol to 20 mL of 2% Cs in acetic acid solution in a 60 °C water bath. Afterwards, the homogeneous solution was casted in a glass mould (5 × 5 cm<sup>2</sup>) followed by solvent evaporation. The glass mould was placed in an oven at 80 °C to remove the solvent. The thickness of the obtained electrolyte film was 180–200 μm. The C-polymer actuator was fabricated by hot-pressing the electrode layer and the electrolyte layer under 20 N at 50 °C for 20 min. Due to the solvent evaporation by the hot-pressing, the typical thickness of the C-polymer film was 200–250 μm, which was smaller than the sum of the two electrode layers and the electrolyte layer. Thus, after the hot-pressing technique, the C-polymer actuator was obtained and is presented in Fig. 1(c).

As shown in Fig. 2(a), when an electric field is applied between two electrode layers, positive and negative charges are injected into the two electrodes separately and provide an electric field for the cation  $\text{BIM}^+$ , which migrates to the cathode, and the anion  $\text{BF}_4^-$ , which moves to the anode. Due to the effects of the gain or loss of ion volume causing volume expansion or contraction in the electrolyte layer [15], large-sized  $\text{BIM}^+$  expands more than the small-sized  $\text{BF}_4^-$ , which causes bending to the anode. The other factor is the resultant electrostatic forces between  $\text{BIM}^+$  and  $\text{BF}_4^-$ , which cause a strain in the electrolyte. Then, the electrode layers undergo opposing strains, and a bending moment is further induced [7, 14, 16]. The corresponding photographs of the C-polymer actuator with positive voltage of 5 V (left), negative voltage of 5 V (right), and no applied voltage confirmed the model in Fig. 2(b).

### Measurement Setup and Methods

The experiments were conducted on a 35 mm × 5 mm strip clipped by two copper power electrodes. The experimented samples were chitosan polymer actuators with various thicknesses of the electrolyte layers and various thicknesses of the electrode layers. The electromechanical properties, including the strain difference, blocking force, etc., were measured at five direct currents (DC). The deflection displacement, at a point 30 mm away (free length) from the fixed point, was continuously monitored from one side of the actuator strip by using a laser sensor (Model FT5070F, accuracy of 0.01 mm), and the blocking force was measured at a point 3 mm away from the tip point by using a force sensor (Model FA1004, accuracy of 0.01 g).

The experimental set-up is shown in Fig. 3, and a signal generator (SP1651 type digital synthesis of low frequency signal generator) was used to activate the C-polymer actuator. The conditioning circuit and the data acquisition card were integrated in the DAQ device. One side was linked with the signal generator and sensors, such as the laser sensor or force sensor, and the other side was transferred to a PC (personal computer) with a communicated interface. The PC was applied to control and communicate between the DAQ device and the software operation platform established by the GUI module in Matlab 2012a. Finally, the data were processed directly using Matlab 2012a.

According to previous research works [32, 33], the transient displacement is transformed into the strain difference ( $\varepsilon$ ) between two electrode layers using the following equations, as shown in Fig. 4. The strain difference can be given by:

$$\varepsilon(L_f, t) = \frac{2 \delta(L_f, t) w}{\delta^2(L_f, t) + L_f^2} \quad (1)$$

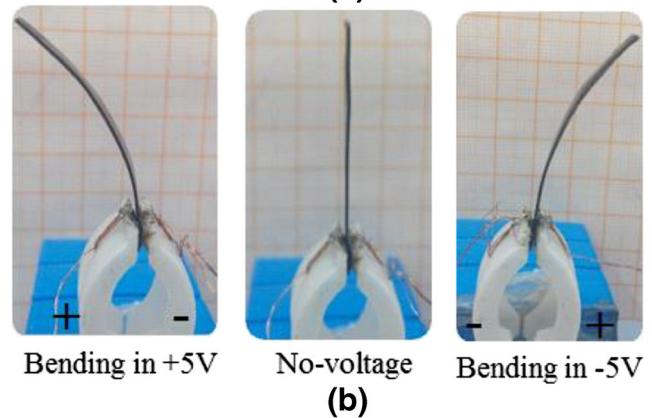
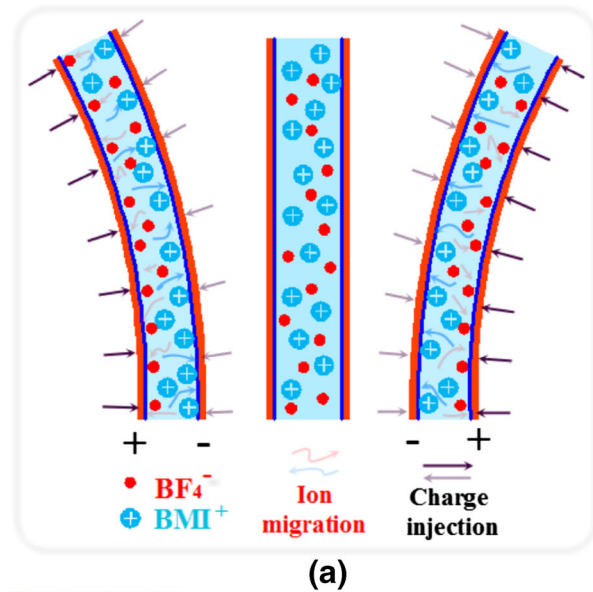


**Fig. 2** (a) Schematic structure of the bending model illustration of the bimorph configured actuator under positive (left), negative (right), and no extra electrical field. (b) The corresponding photographs of C-polymer actuator with a positive (left), negative (right), and no extra electrical field of 5 V direct current, which well confirms with the model

The related transformation relationship is shown in (equation (2)) to (equation (5)). Assuming that the bending slope is fixed, the relationship between the displacement  $\delta$  (mm) and the curvature radius  $R$  (mm) is expressed as:

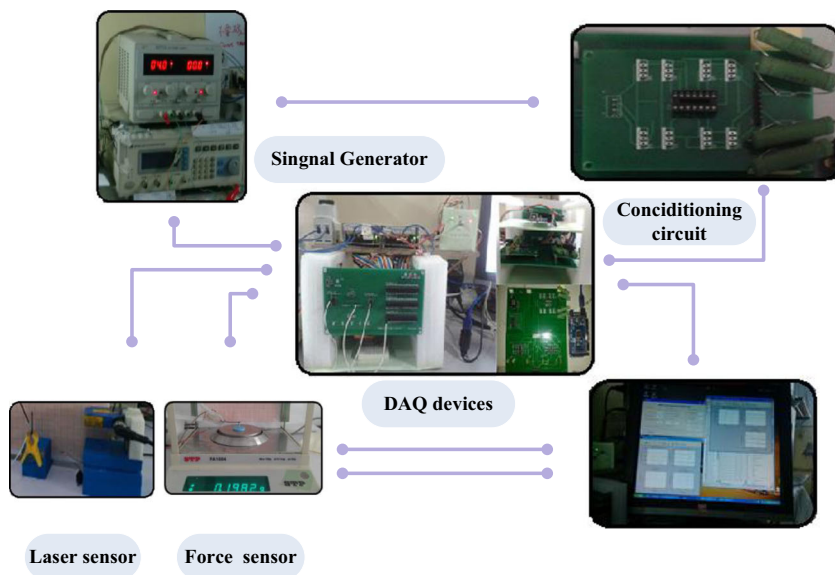
$$R = \frac{\delta^2(L_f, t) + L_f^2}{2w} \quad (2)$$

In the experiment, the clamping side length  $L_f$  (mm) is chosen as a random variable, and the length of the sample is a fixed value  $L$ . The tip displacement  $\delta(L, t)$  (mm) can be represented as:

$$\delta(L, t) = 2R \sin^2\left(\frac{L}{2R}\right) \quad (3)$$

According to the proportion of concentric circles, the relation is available as:

**Fig. 3** Schematic diagram of experiment setup for C-polymer actuator



$$\frac{R-w}{L + \Delta L_1} = \frac{R}{L + \Delta L_2} \tag{4}$$

According to (equation (4)), the bending strain equation is:

$$\varepsilon = \frac{\Delta L_2 - \Delta L_1}{L} = \frac{w}{R} \left( 1 + \frac{\Delta L_2}{L} \right) \tag{5}$$

Where the right side of  $\Delta L_2/L$  is very small and can be ignored.  $L + \Delta L_2$  and  $L + \Delta L_1$  denote the bending length on the left side and right side, respectively.  $w$  is the thickness of the C-polymer actuator.  $t$  is the time variable(s). Five sample displacement measurements were averaged.

The double-layer capacitance of the polymer-supported electrode was estimated by cyclic voltammetry (CV) using a multi-channel chemical test station (Vmp3). Also, the electrode resistance ( $R_1$ ) and the charge transfer resistance ( $R_2$ )

were both obtained by alternating current (AC) impedance testing. All measurement data presented here are an average of five samples.

## Results and Discussion

### C-polymer Actuator with Various Thicknesses of the Electrolyte Film

To confirm the electromechanical properties, we conduct cyclic voltammetry (CV) of the biopolymer chitosan-supported configuration film. Figure 5(a) shows the CV curves of various thicknesses of the electrolyte layer (0.3 mm, 0.8 mm, 1.3 mm) at a sweep rate of 20 mV/s and voltage of  $-1 \text{ V} \sim 1 \text{ V}$ . Thus, the specific capacitance is further applied as shown by (equation (6)):

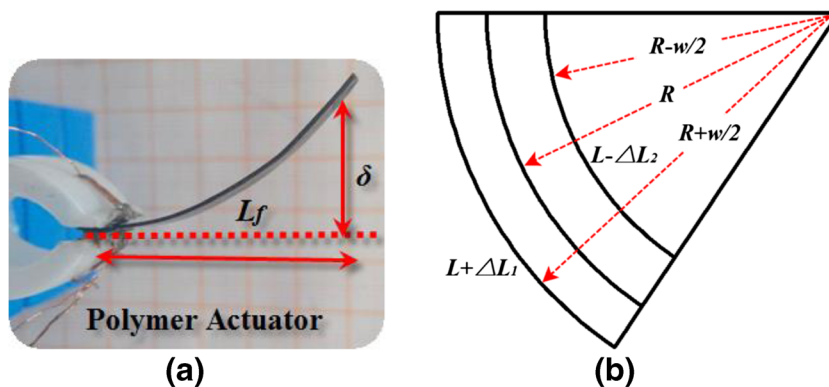


**Fig. 4** (a) the laser displacement measurement for the cantilever bending C-polymer actuator ( $\delta$  is the transient displacement, and  $L_f$  is the length from the fixed ending to the measured ending). (b) Schematic diagram for evaluation of the strain from measured displacement. The relation  $(R-w/2)/(R + w/2) = (L - \Delta L_2)/(L + \Delta L_1)$  can be obtained from the figure, where  $R$  is the curvature radius and  $\Delta L_1$  and  $\Delta L_2$  are the induced change in length for each electrode caused by application of the voltage. From the relation, the stain difference  $\varepsilon (L_f, t)$  is given by  $(2\delta(L_f, t)w)/(\delta^2(L_f, t) + L^2)$ .  $R$  is given by  $(\delta^2(L_f, t) + d^2)/(2w)$ , so that we can obtain (equation (1))



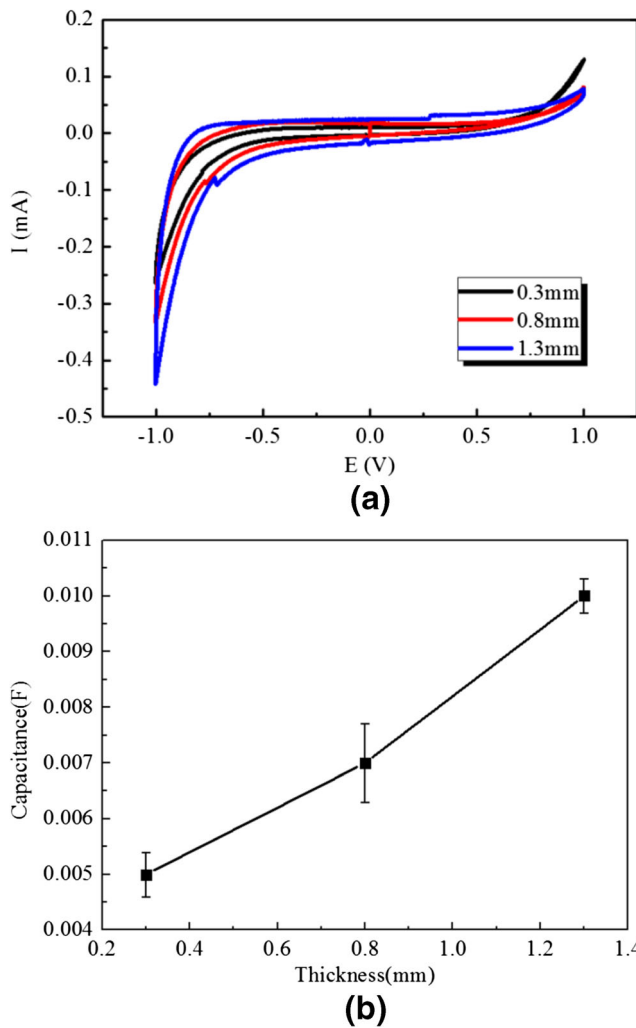


**Fig. 5** (a) CV curves of various thicknesses of the electrolyte layer (0.3 mm, 0.8 mm, 1.3 mm), at sweep rate of 20 mV/s, and voltage of -1 V ~ 1 V. (b) dependence of the capacitance of C-polymer electrolyte under different thicknesses (0.3 mm, 0.8 mm, 1.3 mm)

$$c = \frac{I}{S \times m \times \Delta V} \int_{v_1}^{v_2} idv \quad (6)$$

where *c* is the specific capacitance of the electrode layer (F/g), *S* is the scanning speed of the workstation (V/s), *m* is the quality of the electrode layer immersed in the solution (g),  $\Delta V$  is the potential window (V), *v*<sub>1</sub> and *v*<sub>2</sub> are the scanning voltage values at the beginning and the end (V), respectively, and *i* is the test current (A).

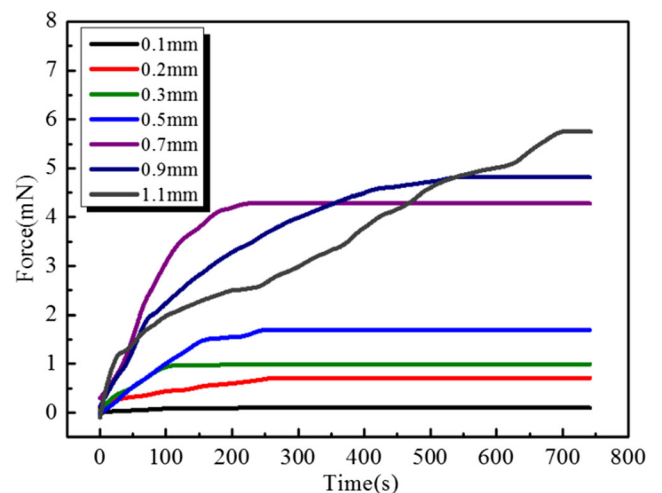
The absolute value of the oxidation peak current and the reduction peak current in the CV curve are equal. This value is always one, which proves that the CV reaction is reversible. Normally, a large CV scanning speed gives a large current of the electrochemical reaction. The positive potential leads to oxygen absorption, and the negative potential leads to hydrogen absorption. Different electrode materials can produce different properties of oxygen potential and hydrogen absorption. This study shows that the film has a larger degree of hydrogen

absorption potential, which indicates that the membrane has a certain overflow of hydrogen and oxygen and that a certain doping substance is needed for improvement. Under the circumstances, a small scanning speed of the CV curves can well reflect the characteristics of the membrane.

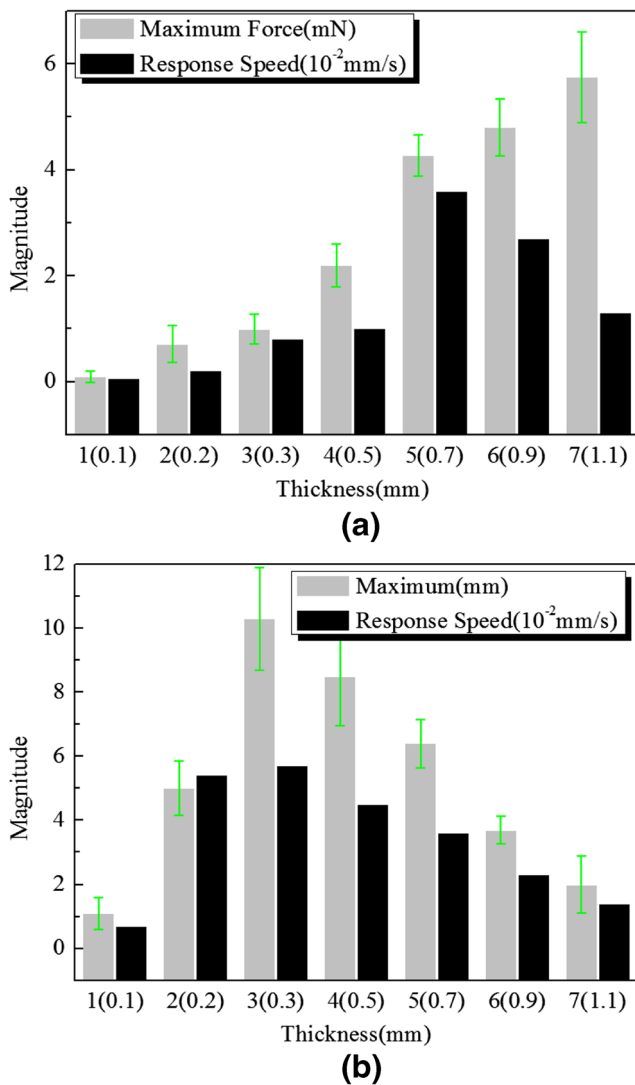
In Fig. 5(b), the capacitances of the electrolyte layer with various thicknesses of 0.3 mm, 0.8 mm, and 1.3 mm are 0.005 F, 0.007 F, and 0.01 F, respectively. Clearly, the capacitance value for a 1.3 mm thick electrolyte film is 20 times greater than that of the 0.3 mm thick film. Moreover, it is clear that the thickness of the electrolyte film has a great influence on its capacitance.

Figure 6 shows the change in the blocking force with time for different thicknesses of the electrolyte layer (0.1 mm, 0.2 mm, 0.3 mm, 0.5 mm, 0.7 mm, 0.9 mm, and 1.1 mm). It can be discovered that the blocking force increases with the increase in the thickness of the electrolyte film, and the maximum blocking force at the thickness of 1.1 mm of the C-polymer actuator is 63.9 times larger than that at the thickness of 0.1 mm. After handling, a curvature, which is approximately a linear fit, is applied to explain the response speed appearing in Fig. 7(a). It is shown that the changing rules are different from the maximum blocking force value. We can note that the response speed at the thickness of 0.7 mm has a peak value of 0.027 mN/s, which is significantly greater than that for the others. Hence, the results verify that an increasing thickness of the electrolyte layer will generate an enhancement of the blocking force and the response speed, which also presents a peak value of the response speed.

The maximum displacement value and the response speed at the thicknesses of 0.1 mm, 0.2 mm, 0.3 mm, 0.5 mm, 0.7 mm, 0.9 mm, and 1.1 mm are further summarized in Fig. 7(b). Interestingly, different from the blocking force, it can be discovered that the increasing trends are similar to the



**Fig. 6** The blocking force changing with time under different thicknesses of electrolyte layer (0.1 mm, 0.2 mm, 0.3 mm, 0.5 mm, 0.7 mm, 0.9 mm, 1.1 mm)



**Fig. 7** (a) The maximum blocking force value and response speed under various thicknesses of electrolyte layer (1–0.1 mm, 2–0.2 mm, 3–0.3 mm, 4–0.5 mm, 5–0.7 mm, 6–0.9 mm, 7–1.1 mm). (b) The maximum displacement value and response speed under various thicknesses of electrolyte layer (1–0.1 mm, 2–0.2 mm, 3–0.3 mm, 4–0.5 mm, 5–0.7 mm, 6–0.9 mm, 7–1.1 mm)

response speed of the blocking force with time. That is, with the increase in the electrolyte thickness, there is a peak value of the maximum displacement (10.3 mm) and the response speed (0.057 mm/s) appearing at the thickness of 0.3 mm. Thus, it is shown that the displacement value is largely attributed to the stiffness of the electrolyte layer, and a thick electrolyte film has bad flexibility, which obviously restrains the deflection.

The main reason for the bending force increasing with the thickness can be explained from different aspects. From the perspective of internal ion movement, the increase in thickness will change the internal impedance. The larger thicknesses of the C-polymer actuator are accompanied by better

internal conductive properties, which lead to improved conduction velocities of movement ions. At the same time, this problem can be explained from the aspect of electromechanical energy density. The energy density of the active phase will stay the same, and more materials will generate a larger response.

However, with the increase in the thickness of the C-polymer actuator, the response speed of the output force increases after the first drop. The main reasons can be explained from the perspective of mechanics analysis. Through bending deformation, the C-polymer actuator touches the force sensor, and the output force is tested. During the bending process, certain internal stress constraints need to be overcome. When the membrane thickness is small, the surface stress constraints of the C-polymer are small enough to overcome, and the response speed of the output force presents an increasing trend. When the membrane thickness is increased to a certain value, the output force is not enough to overcome its own stress constraint, and the response speed presents a reducing tendency.

By using (equation (1)), the measured displacement ( $\delta$ ) is transformed into a strain difference ( $\epsilon$ ) between the two electrode layers on the assumption that the cross-sections are planes at any position along the actuator, and there is no distortion of the cross-sections. Figure 8(a) shows the generated strains ( $\epsilon$ ) for various thicknesses of the electrolyte layer at the applied direct current of 5 V. After processing, the maximum strain differences ( $\epsilon$ ) of the polymer-supported C-polymer actuator with various thicknesses of the electrolyte layer (1–0.1 mm, 2–0.2 mm, 3–0.3 mm, 4–0.5 mm, 5–0.7 mm, 6–0.9 mm, and 7–1.1 mm) are presented in Fig. 8(b). At the same time, an initial growing and then reducing trend is observed, and a peak strain difference (0.493%) appears for the thickness of 0.3 mm. Although the strain values seem to be very small, the effects on the electromechanical properties are remarkable. Thus, it is considered that the thickness factors are important in the generated strain of the C-polymer actuator. The experimental results show that the values of the strain are weak and keep within 0.5%. Also, an optimum point exists for the membrane layer thickness of 0.3 mm. This shows that large strain changes are observed on the surface of the C-polymer actuator under large deflection deformation. It can be considered that the displacement corresponds to the change in strain. Therefore, an optimum point exists for the generated strain and displacement.

### C-polymer Actuator with Various Thicknesses of the Electrode Film

After the testing methods, the CV curves of various thicknesses of the electrode layer (0.15 mm, 0.2 mm, and 0.25 mm) at a sweep rate of 50 mV/s and voltage of  $-0.5$  V  $\sim$  0.5 V are presented in Fig. 9(a). Here, the content ratio of MCNTs and chitosan of the electrode layer is selected as 3:2. An increasing

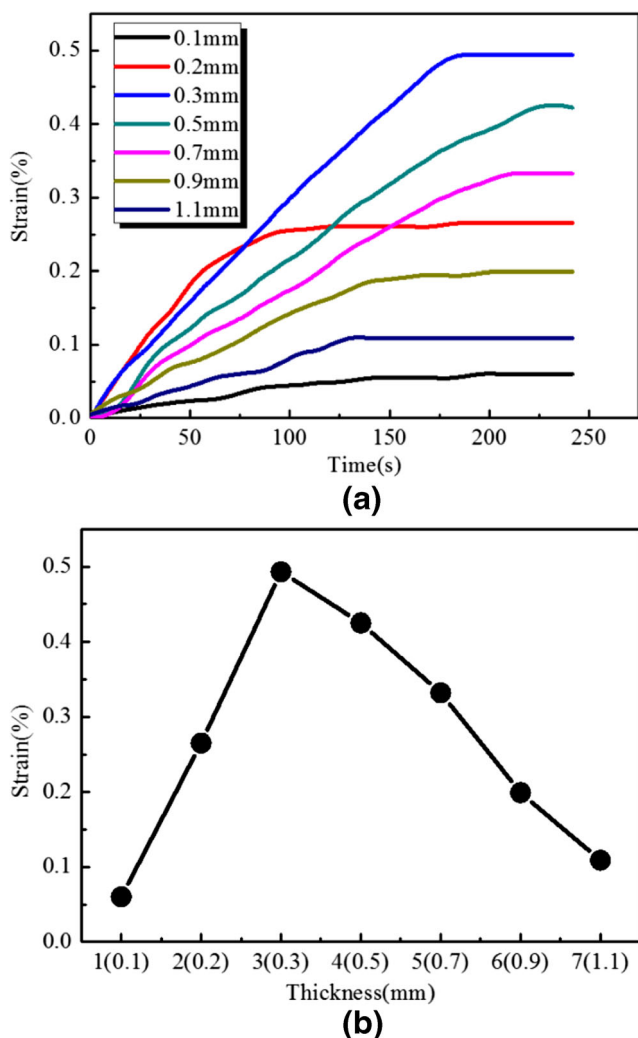


**Fig. 8** (a) the curves of the strain difference ( $\epsilon$ ) of the polymer-supported C-polymer actuator under the applied voltage of 5 V. (b) the maximum strain difference ( $\epsilon$ ) of polymer-supported C-polymer actuator under various thickness electrolyte layer (1–0.1 mm, 2–0.2 mm, 3–0.3 mm, 4–0.5 mm, 5–0.7 mm, 6–0.9 mm, 7–1.1 mm)

trend is observed with the increase in thickness in the electrode film. The specific capacitance and capacitance of the C-polymer electrode with different thicknesses (0.15 mm, 0.2 mm, and 0.25 mm) are shown in Fig. 9(b). It is clear that the curves of the specific capacitance and capacitance both exhibit a linear increase. Clearly, the specific capacitance and capacitance at the electrode film thickness of 0.25 mm are 1.23 times and 3.64 times greater, respectively, than that of the 0.15 mm thick film. It is clear that the thickness of the electrode layer has a great influence on its capacitance value. Therefore, a larger thickness of the electrode layer, which causes a large capacitance, is beneficial for electronic storage.

The reasons of the increased thickness of the electrode layer enhancing the capacitance of the device can be explained as follows. With the increase in the thickness of the electrode layer, the amount of the conductive agent of multi-walled

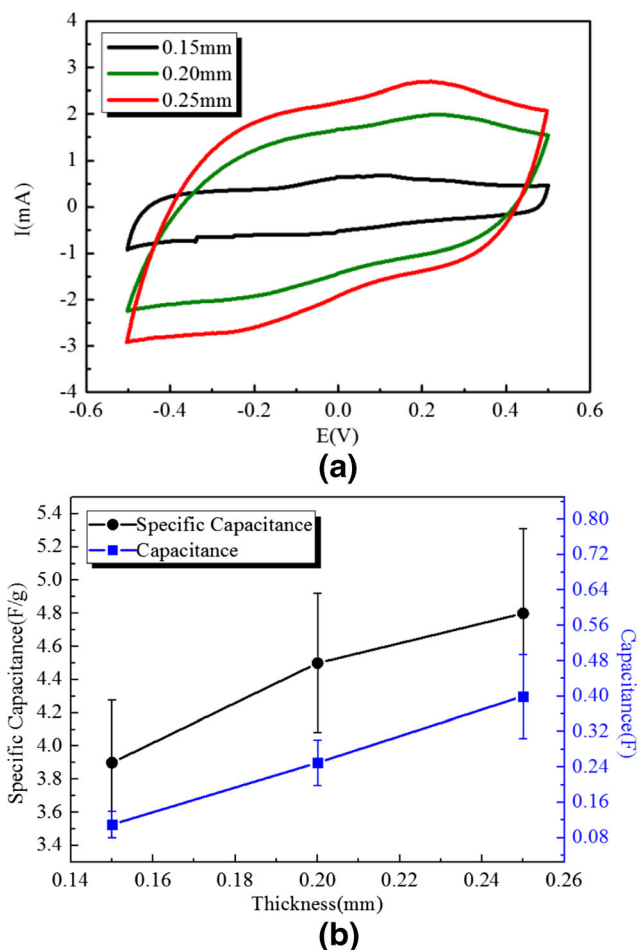


**Fig. 9** (a) CV curves under various thickness of the electrode layer (0.15 mm, 0.2 mm, 0.25 mm), at sweep rate of 50 mV/s and voltage of  $-0.5$  V– $0.5$  V. (60% MCNTs) (b) Dependence of the capacitance of C-polymer electrode under different thickness (0.15 mm, 0.2 mm, 0.25 mm)

carbon nanotubes (MCNTs) is also increased. MCNTs exhibit fragmented distribution in the electrode layer. Its larger content produces a greater internal clutter dispersion of the electrode layer. The interior capacitance of the electrode layer depends on the specific surface area. A more disorderly dispersion of the electrode layer can generate a larger specific surface area. This greatly improves the efficiency of the conductive electrode layer.

Figure 10 shows the alternating current (Ac) impedance curves for thicknesses of 0.15 mm, 0.2 mm, and 0.25 mm. The signal amplitude is set as 5 mV, and the frequency is in the range of 100 KHz ~ 10 MHz. An equivalent circuit model involving the resistance and capacitance is applied to calculate the resistance value. As seen in Fig. 10(a), in the equivalent circuit model,  $R_{ii}$  is regarded as the solution resistance, and  $C_d$  is the double-layer capacitance, while  $R_{ct}$  is seen as the resistance for transferring the charges. When the frequency tends to infinity, the capacitors for high frequency hindering can approximately approach zero, and the measured value of  $R_{ii}$

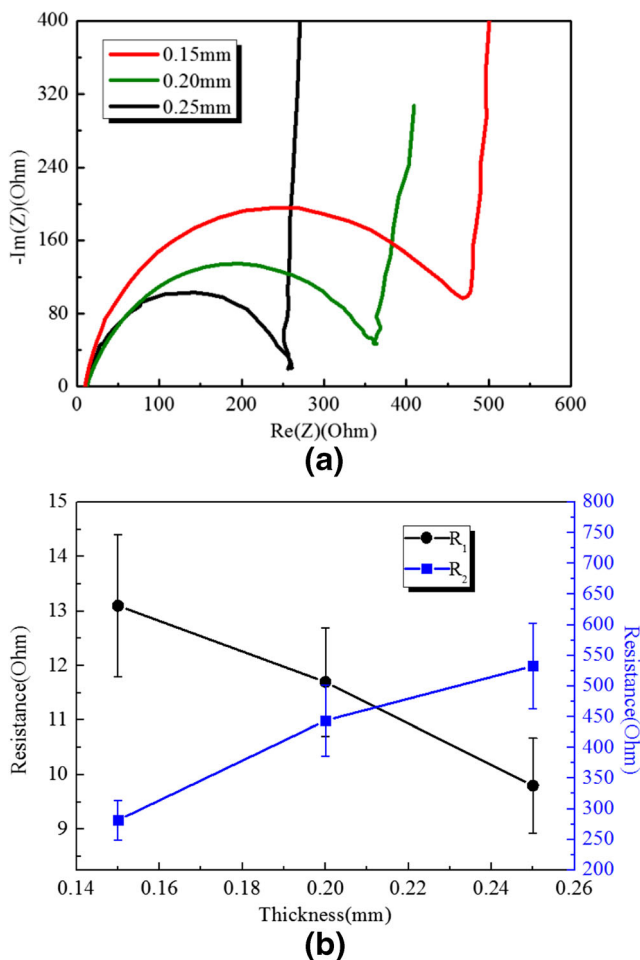


**Fig. 10** (a) Ac impedance curves of various thickness electrode layer, at 5 mV 100KHz-10 MHz (0.15 mm, 0.2 mm, 0.25 mm). (b) Dependence of the resistance of the C-polymer actuator electrode layer (0.15 mm, 0.2 mm, 0.25 mm)

can be treated as the system resistance, which is regarded as the resistance of the electrode film. Moreover, when the frequency approaches zero, the measured resistance value is the sum of  $R_{ci}$  and  $R_{ct}$ .

The charge transfer resistance  $R_2$  and the electrode resistance  $R_1$  are both shown in Fig. 10(b). The electrode resistance  $R_1$  decreases with increasing thickness of the electrode layer. On the contrary, the charge transfer resistance  $R_2$  increases with increasing thickness of the electrode layer. For different thicknesses of the electrode film, i.e., 0.15 mm, 0.2 mm, and 0.25 mm, the electrode resistance  $R_1$  is 13.1  $\Omega$ , 11.7  $\Omega$ , and 9.8  $\Omega$ , respectively, while the charge transfer resistance  $R_2$  is 281.3  $\Omega$ , 443.8  $\Omega$ , and 532.6  $\Omega$ , respectively. The resistance  $R_1$  for a thickness of 0.25 mm is 1.34 times smaller than that for a thickness of 0.15 mm. We can consider that the effects of the changing resistance are significant.

Figure 11 shows the blocking force changing with time for various thicknesses of 0.15 mm, 0.2 mm, and 0.25 mm. It is clearly discovered that the blocking force increases with

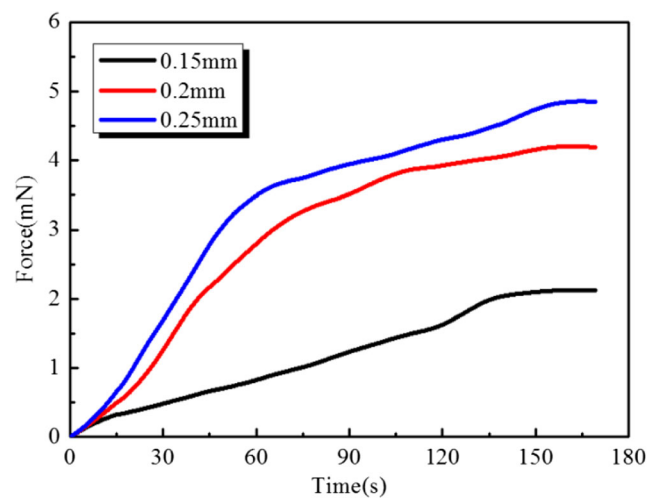


**Fig. 11** the blocking force changing with time under different thickness of electrode layer (0.15 mm, 0.2 mm, 0.25 mm)

increasing thickness of the electrode layer, and the maximum blocking force for a thickness of 0.25 mm of the C-polymer actuator is 2.19 times larger than that for the thickness of 0.15 mm, as shown in Fig. 12(a). Then, a curvature, which is approximately a linear fit, is also applied to estimate the response speed appearing in Fig. 12(a). It is exhibited that the changing rules are almost similar with the maximum blocking force value, and the response speed for the thickness of 0.25 mm of the C-polymer actuator is 5.00 times larger than that for the thickness of 0.15 mm. Obviously, increasing the thickness of the electrode layer will generate an enhancement of the blocking force and the response speed.

Figure 12(b) shows the curves of the maximum displacement value and the response speed at thicknesses of 0.15 mm, 0.2 mm, and 0.25 mm. It can be found that with increasing thickness of the electrode layer, the maximum displacement value and the response speed of the C-polymer actuator are 6.04 times and 20.00 times smaller than that for the thickness of 0.15 mm, respectively. We can observe that the effects on the displacement of the electrode layer with various thicknesses are obviously larger than those on the blocking force. Therefore, we acknowledge that the output blocking force can be improved to some extent, while the flexibility properties of the electrode layer are very significant for increasing the displacement value.

Similar to the methods of the electrolyte layer above, the measured displacement ( $\delta$ ) under various thicknesses of the electrode layer is transformed into the strain difference ( $\epsilon$ ) between two electrode layers. Figure 13 shows the generated strains ( $\epsilon$ ) of the electrode layer with various thicknesses at the applied direct current of 5 V. The generated strain values under various thicknesses of 0.15 mm, 0.2 mm, and 0.25 mm are 0.59%, 0.36%, and 0.12%, respectively. Obviously, the generated strain of 0.15 mm thickness is 4.92 times greater than



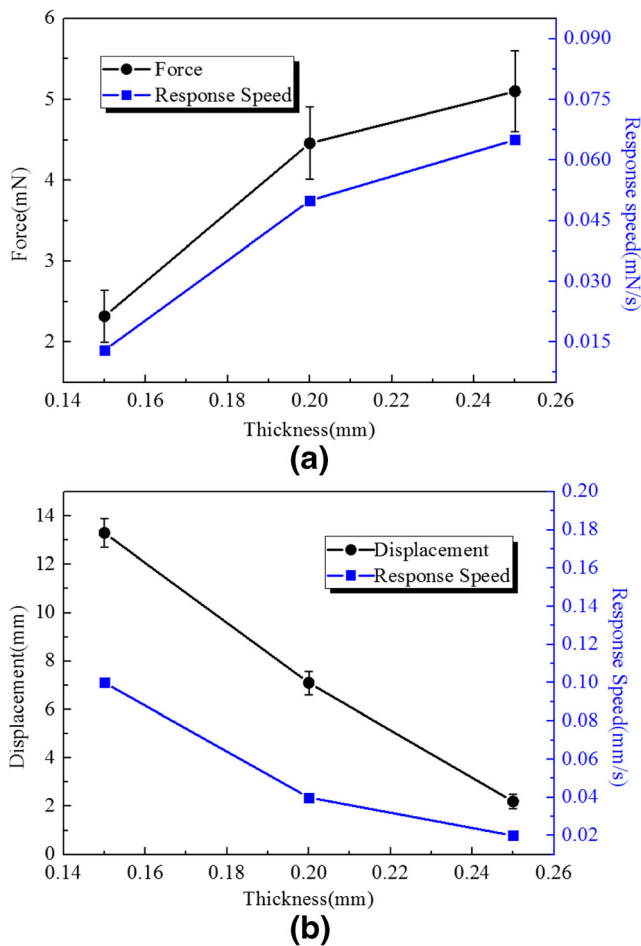


**Fig. 12** (a) the maximum blocking force value and the response speed under various thicknesses of electrode layer (0.15 mm, 0.2 mm, 0.25 mm). (b) the maximum displacement value and the response speed under various thickness of electrode layer (0.15 mm, 0.2 mm, 0.25 mm)

that of 0.25 mm thickness. Therefore, this means that the increasing thickness of the electrode layer is against the strain

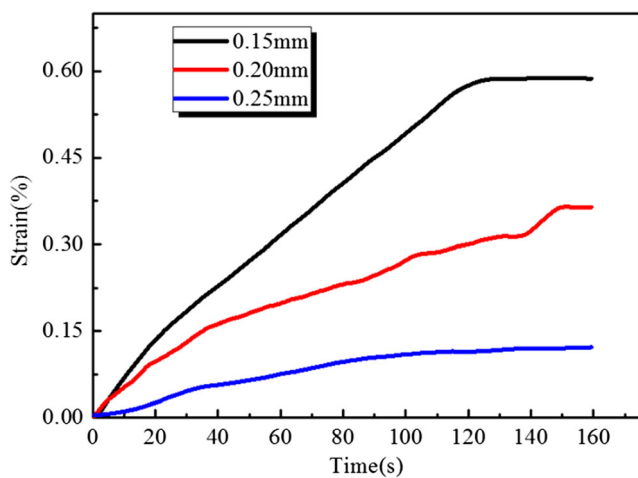


**Fig. 13** the strain difference under various thickness of electrode layer (0.15 mm, 0.2 mm, 0.25 mm)

difference on the electrode surface due to the growing stiffness of the electrode layer.

**Efficiency of the C-polymer Actuator with Various Thicknesses of the Electrode Film**

To further study the effects of various thicknesses of the electrode layer (0.15 mm, 0.2 mm, and 0.25 mm), the electromechanical energy efficiency is obtained by using the CV curves at a sweep rate of 50 mV/s and voltage of -0.5 V ~ 0.5 V in Fig. 9(a). According to Jung et al. [8], the electromechanical efficiency of a C-polymer actuator can be defined as:

$$\eta = \frac{\bar{T}_{C-polymer}}{\bar{E}_{input}} = \frac{\left(\int_0^L \frac{1}{2} \rho \Phi^2(x) dx\right) \left(\int_0^T (2\pi f_{ex})^2 \cos^2(2\pi f_{ex}t) dt\right) (\delta^2_{max})}{A \bar{E}_{input} (\delta^2_{max})} = C \frac{\bar{E}_{input}}{\bar{E}_{input}} \tag{7}$$

where C is a constant for all actuators.  $\bar{E}_{input}$  is the dissipated electrical input energy, and  $\delta_{max}$  is the maximum tip displacement, which are given by the following equations.

$$\bar{E}_{input} = \frac{E_{input}}{A} = \frac{\int_0^T i(t)v(t)dt}{A} = \frac{1}{f_{ex}} \int_0^{1/f_{ex}} \frac{i(t)}{A} V_{input} \sin(2\pi f_{ex}t) dt \tag{8}$$

where A, i, v, T,  $f_{ex}$ , and  $V_{input}$  are the area of electrode, measured current, input voltage, period, frequency, and voltage input, respectively. The kinetic energy stored in the C-polymer actuators for a cycle can be computed from the following equation:

$$\bar{T}_{C-polymer} = \frac{T_{C-polymer}}{A} = \frac{\int_0^T \int_0^L \frac{1}{2} \rho \left(\frac{dw(w,t)}{dt}\right)^2 dx dt}{A} \tag{9}$$

where  $\rho$  and  $w(x, t)$  are the equivalent density per length and the transverse displacement, respectively. Thus, the separation of variables can be expressed by a mode shape of a cantilever beam,  $\Phi(x)$ , and the time-dependent function,  $f(t)$  [34]. Moreover,  $w(x,t)$  can be further calculated as  $\omega(x, t) = \delta(x)f(t) = \delta_{max}\Phi(x) \sin(2\pi f_{ex}t)$ .

**Table 1** Electromechanical energy efficiency of C-polymer actuator at sweep rate of 50 mV/s and voltage of  $-0.5\text{ V} \sim 0.5\text{ V}$ 

Membrane thickness(mm)		Electrical input energy density $\bar{E}_{input}$ (mJ/mm <sup>2</sup> )	Maximum tip displacement $\delta_{max}$ (mm)	Specific electromechanical energy efficiency rate
Electrolyte layer	Electrode layer			
0.3000	0.1500	0.9436	13.3000	1.0000
0.3000	0.2000	2.1445	7.1000	0.1254
0.3000	0.2500	3.4313	2.2000	0.0995
0.8000	0.1500	0.0600	5.9000	2.8135
1.3000	0.1500	0.0858	1.7000	0.1797

Here, the electromechanical energy efficiency of the C-polymer actuator with various thicknesses of the electrode layer can be defined in the following form:

$$\frac{\eta_{\text{various-thickness}}}{\bar{\eta}} = \frac{\eta_{\text{various-thickness}}}{\eta^{0.15\text{mm}}} = \left( \frac{\delta_{\text{max}}^{\text{various-thickness}}}{\delta_{\text{max}}^{0.15\text{mm}}} \right)^2 \left( \frac{\bar{E}_{\text{input}}^{0.15\text{mm}}}{\bar{E}_{\text{input}}^{\text{various-thickness}}} \right) \quad (10)$$

Actually, a larger tip displacement means the generation of a much higher kinetic energy in the oscillating cantilever actuator, and a higher kinetic energy requires external work from the electrical input. Thus, the dissipated electrical input energy densities of our C-polymer actuator can be calculated by using (equation (7)), which will be the same as the area of the curves in Fig. 9(a). The maximum displacement of the C-polymer actuator with various membrane thicknesses and the values of the electrical input energy per unit area are listed in Table 1.

As shown in Table 1, the electromechanical energy efficiency of the C-polymer actuator with various thicknesses of the electrode layer and the electrolyte layer obviously decreases in the current conditions. Based on the electromechanical energy efficiency of the C-polymer actuator with a fixed thickness of 0.3 mm for the electrolyte layer and 0.15 mm for the electrode layer, the specific electromechanical energy efficiency of the C-polymer actuator with different thicknesses is studied. With the increase in the thickness of the electrode layer, the specific electromechanical energy efficiency shows a declining trend. Due to the smaller thickness of the electrode layer, the surface strain is small. The increase in the thickness of the C-polymer actuator can improve the conductive efficiency of the electrode layer. Therefore, it can significantly reduce the energy consumption of the C-polymer actuator. On the other hand, with the increase in thickness of the electrolyte layer, the specific electromechanical energy efficiency presents a rise after falling. With the increase in thickness of the electrolyte layer, the conductive efficiency of the internal ions is enhanced. However, for larger thicknesses

of the electrolyte layer, large energy consumption for the C-polymer actuator is required to overcome its internal stress. With the increase in the electrolyte layer thickness, the C-polymer actuator becomes a capacitor, and the energy dissipation is stored. Thus, there is a reduced energy consumption of the electromechanical energy efficiency.

## Conclusions

In summary, a highly biocompatible polymer actuator, which consisted of multi-walled carbon nanotube (MCNT) film as the double electrode layer and an electrolyte layer equipped with a chitosan polymer skeleton and ionic liquid was developed. In this manuscript, the electromechanical properties of the C-polymer actuator, involving the blocking force, displacement, generated strain, and response speed, obviously depended on the various thicknesses of the electrode layer and the electrolyte layer. From the analysis of cyclic voltammetry (CV) and alternating current (AC), we explained the electromechanical properties of the C-polymer actuator, and the thickness factors can dramatically affect the electrochemical parameters, such as the resistance and the capacitance. Furthermore, the generated strain of the 0.15 mm thick film (59%) was 4.92 times greater than that of the 0.25 mm thick film, which was against the strain difference on the electrode surface due to the growing stiffness of the electrode layer. More importantly, the electromechanical energy efficiency results demonstrated that the thicknesses of the electrode layer and the electrolyte layer will cause the dissipation of electric energy, and our actuator exhibited excellent electromechanical energy efficiency under a high electrical conductivity of the electrode layer, which can enhance the specific electromechanical energy up to 9.95%.

**Acknowledgements** We gratefully acknowledge the financial support from the National Natural Science Foundation of China (31470714), and the Fundamental Research Funds for the Central Universities (2572017BB08).



## References

- Inganäs O, Lundström I (1999) Carbon nanotube muscles. *Science* 284(5418):1281–1282
- Jager EWH, Smela E, Inganäs O (2000) Microfabricating conjugated polymer actuators. *Science* 290(5496):1540–1545
- Zhang QM, Li H, Poh M (2002) An all-organic composite actuator material with a high dielectric constant. *Nature* 419(6904):284–287
- Ma M, Guo L, Anderson DG (2013) Bio-inspired polymer composite actuator and generator driven by water gradients. *Science* 339(6116):186–189
- Yu Y, Nakano M, Ikeda T (2003) Photomechanics: directed bending of a polymer film by light. *Nature* 425(6954):145–145
- Enikov ET, Seo GS (2005) Experimental analysis of current and deformation of ion-exchange polymer metal composite actuators. *Exp Mech* 45(4):383–391
- Mukai K, Asaka K, Sugino T (2009) Highly Conductive Sheets from Millimeter-Long Single-Walled Carbon Nanotubes and Ionic Liquids: Application to Fast-Moving, Low-Voltage Electromechanical Actuators Operable in Air. *Adv Mater* 21(16):1582–1585
- Jung JH, Jeon JH, Sridhar V (2011) Electro-active graphene-Nafion actuators. *Carbon* 49(4):1279–1289
- Friend RH, Gymer RW, Holmes AB (1999) Electroluminescence in conjugated polymers. *Nature* 397(6715):121–128
- Palmre V, Hubbard JJ, Fleming M (2012) An IPMC-enabled bio-inspired bending/twisting fin for underwater applications. *Smart Mater Struct* 22(1):014003
- Fennimore AM, Yuzvinsky TD, Han WQ (2003) Rotational actuators based on carbon nanotubes. *Nature* 424(6947):408–410
- Lv S, Dudek DM, Cao Y (2010) Designed biomaterials to mimic the mechanical properties of muscles. *Nature* 465(7294):69–73
- Chaikof EL (2010) Materials science: Muscle mimic. *Nature* 465(7294):44–45
- Lu L, Liu J, Hu Y (2012) Highly stable air working bimorph actuator based on a graphene nanosheet/carbon nanotube hybrid electrode. *Adv Mater* 24(31):4317–4321
- Li J, Ma W, Song L (2011) Superfast-response and ultrahigh power density electromechanical actuators based on hierarchical carbon nanotube electrodes and chitosan. *Nano Lett* 11(11):4636–4641
- Lu L, Chen W (2010) Biocompatible composite actuator: a supramolecular structure consisting of the biopolymer chitosan, carbon nanotubes, and an ionic liquid. *Adv Mater* 22(33):3745–3748
- Kim J, Wang N, Chen Y (2007) Effect of chitosan and ions on actuation behavior of cellulose–chitosan laminated films as electro-active paper actuators. *Cellulose* 14(5):439–445
- Yoshioka Y, Calvert P (2002) Epoxy-based electroactive polymer gels. *Exp Mech* 42(4):404–408
- Spinks GM, Shin SR, Wallace GG (2006) Mechanical properties of chitosan/CNT microfibers obtained with improved dispersion. *Sensor Actuat B-Chem* 115(2):678–684
- Li MC, Zhang Y, Cho UR (2014) Mechanical, thermal and friction properties of rice bran carbon/nitrile rubber composites: Influence of particle size and loading. *Mater Design* 63:565–574
- Richard C, Balavoine F, Schultz P (2003) Supramolecular self-assembly of lipid derivatives on carbon nanotubes. *Science* 300(5620):775–778
- Tu X, Manohar S, Jagota A (2009) DNA sequence motifs for structure-specific recognition and separation of carbon nanotubes. *Nature* 460(7252):250–253
- Harrison BS, Atala A (2007) Carbon nanotube applications for tissue engineering. *Biomaterials* 28(2):344–353
- Liu Y, Tang J, Chen X (2005) Decoration of carbon nanotubes with chitosan. *Carbon* 43(15):3178–3180
- Carson L, Kelly-Brown C, Stewart M (2009) Synthesis and characterization of chitosan–carbon nanotube composites. *Mater Lett* 63(6):617–620
- Çilingir HD, Papila M (2010) “Equivalent” Electromechanical Coefficient for IPMC Actuator Design Based on Equivalent Bimorph Beam Theory. *Exp Mech* 50(8):1157–1168
- Cantrell JT, Ifju PG (2015) Experimental characterization of unimorph shape memory polymer actuators incorporating transverse curvature in the substrate. *Exp Mech* 55(8):1395–1409
- Lu L, Chen W (2011) Supramolecular self-assembly of biopolymers with carbon nanotubes for biomimetic and bio-inspired sensing and actuation. *Nano* 3(6):2412–2420
- Fukushima T, Kosaka A, Ishimura Y (2003) Molecular ordering of organic molten salts triggered by single-walled carbon nanotubes. *Science* 300(5628):2072–2074
- Fukushima T, Asaka K, Kosaka A (2005) Fully Plastic Actuator through Layer-by-Layer Casting with Ionic-Liquid-Based Bucky Gel. *Angew Chem Int Ed* 44(16):2410–2413
- Fukushima T, Kosaka A, Yamamoto Y (2006) Dramatic effect of dispersed carbon nanotubes on the mechanical and electroconductive properties of polymers derived from ionic liquids. *Small* 2(4):554–560
- Sun Z, Zhao G, Guo H (2015) Investigation into the actuating properties of ionic polymer metal composites using various electrolytes. *Ionics* 21(6):1577–1586
- Takeuchi I, Asaka K, Kiyohara K (2009) Electromechanical behavior of fully plastic actuators based on bucky gel containing various internal ionic liquids. *Electrochim Acta* 54(6):1762–1768
- Oh IK, Jung JH, Jeon JH (2010) Electro-chemo-mechanical characteristics of fullerene-reinforced ionic polymer–metal composite transducers. *Smart Mater Struct* 19(7):075009